

M onopole Clustering and Color Con nement in the M ulti-Instanton System

M . Fukushima, H . Suganuma and H . Toki

Research Center for Nuclear Physics, O saka U niversity,
10-1 M ihogaoka, Ibaraki, O saka, 567-0047, Japan

A bstract

We study color con nement properties of the multi-instanton system, which is assumed to carry the essence of the nonperturbative QCD vacuum. We also investigate the feature of monopoles by taking the maximally abelian gauge considering the correspondence between the monopole and the instanton. The feature of monopole trajectories changes drastically with the instanton density. At the high instanton density, there appears one very long and highly complicated monopole loop covering the entire physical space. In order to clarify the infrared properties, we make the "block-spin" transformation for the monopole currents. The appearance of a global network of long monopole loops resembles the lattice results in the con nement phase. Furthermore, we observe that the SU (2) Wilson loop obeys the area law in the multi-instanton system. The string tension of this system directly relates with the instanton density. The multi-instanton system provides about 0.4 GeV = fm at a density of about $(N = V) = (1 = fm)^4$, where the averaged instanton size is $= 0.4 fm$.

1 Introduction

Quantum chromodynamics (QCD) has been established as the fundamental theory of the strong interaction. In the ultraviolet region, perturbative QCD provides a systematic method in describing the high-energy experimental data due to the asymptotic freedom. On the other hand, there appear various nonperturbative phenomena as color confinement, dynamical chiral symmetry breaking and the $U_A(1)$ anomaly in the infrared region. Since the QCD vacuum is composed of gluon fields interacting in a highly complicated way, it is hard to understand these properties from perturbative points of view.

There appear two non-trivial topological objects, instantons and monopoles, which are caused by the presence of self-interactions of the nonabelian gauge field. These topological objects may provide a useful approach for descriptions of the QCD vacuum, where color confinement is realized and the chiral symmetry is spontaneously broken. Above the critical temperature, such topological excitations disappear and then, the nonperturbative vacuum changes into the perturbative one [1], where the deconfinement phase transition happens and the chiral symmetry is restored.

In 1981, 't Hooft proposed the abelian gauge, where color-magnetic monopoles appear as a relevant degree of freedom for the description of color confinement [2]. In the abelian gauge, the $SU(N_c)$ nonabelian gauge theory is reduced to the $U(1)^{N_c-1}$ abelian gauge theory with color-magnetic monopoles. The appearance of magnetic monopoles corresponds to a homotopy group, $\pi_2(SU(N_c)) = U(1)^{N_c-1} = Z_1^{N_c-1}$. Namely, 't Hooft and Mandelstam suggested that the color confinement mechanism is caused by the dual Meissner effect with monopole condensation in a suitable abelian gauge, which is a dual version of Cooper pair condensation in the ordinary superconductivity [3, 4, 5]. On the other hand, because of the recent computational progress, the lattice

QCD simulation becomes a powerful approach to understand the nonperturbative QCD vacuum. This method has allowed to extract some relevant degrees of freedom for characteristic features of QCD [6]–[12]. It is found by the lattice QCD that a very long and highly complicated monopole loop covers the entire physical vacuum corresponding to monopole condensation at the constituent phase. The abelian dominance, where the abelian degrees of freedom including monopoles are relevant for the nonperturbative nature, was demonstrated then by analytical and lattice studies [13, 14]. Recently, it is believed that monopole condensation plays an essential role on color constituent and chiral-symmetry breaking [15]–[17].

The instanton configuration discovered in 1975 by Belavin, Polyakov, Shvarts and Tyupkin [18] is a classical and self-dual solution of the Euclidean field equation in the Yang-Mills theory. The appearance of instantons corresponds to another homotopy groups, $\pi_3(SU(N_c)) = \mathbb{Z}_1$ [19], which is different from that of magnetic monopoles. In the Minkowski space, the instanton is interpreted as the tunneling phenomenon among the degenerate vacua which are labeled by different winding numbers. In order to extract the instanton from the QCD vacuum numerically, it is useful to apply a cooling technique, which minimizes the local action and removes short-range quantum fluctuations [20, 21]. In the QCD vacuum, there exist many topological objects like instantons and anti-instantons with a density about $(1/fm)^4$. The instanton is important for nonperturbative phenomena related to the $U_A(1)$ anomaly [22] and the large $^0 m$ mass. In 1979, Witten and Veneziano indicated an approximate relation between the $^0 m$ mass and the topological susceptibility [23, 24]. Also chiral-symmetry breaking could be interpreted as the instanton effect [25]. However, until now, there has been no evidence that instantons have anything to do with color constituent in the 4-dimensional gauge theory, although Polyakov discovered that instantons cause constituent in certain 3-dimensional Georgi-Glashow models [26].

Recent studies show remarkable facts that instantons are directly related to monopoles [27]–[38] in the abelian gauge, although these topological objects belong to different homotopy group. Such correlations indicate that instantons may be important for the promotion of long monopole loops, which is identified as a signal of monopole condensation. Therefore, we take the multi-instanton system in order to clarify monopole clustering and constituent properties in terms of instantons.

2 Topological Objects in the QCD Vacuum

In this section, we briefly review two topological objects as instantons and monopoles in the QCD vacuum.

The instanton is a classical and non-trivial solution of the Euclidean Yang-Mills theory, whose action is written as

$$S = \frac{1}{2g^2} \int d^4x G^a G^a : \quad (1)$$

Here, in order to make the notation and the discussion simpler, we take the SU(2) case and represent $A^a(x) = ig\frac{a}{2}A^a(x)$ and $G^a(x) = ig\frac{a}{2}G^a(x)$, which are defined as the antihermite variables. In order to find a topological solution, the Yang-Mills action is rewritten as

$$S = \frac{1}{8g^2} \int d^4x f G^a G^a g^2 - \frac{8\pi^2}{g^2} Q ; \quad (2)$$

by using the dual field strength $G^a = \frac{1}{2} \epsilon^{abc} G^b G^c$. Here, the topological charge is defined as $Q = \frac{1}{32\pi^2} \int d^4x f G^a G^a g^2$, which corresponds to the winding number of the homotopy group, $\pi_3(SU(N_c)) = \mathbb{Z}_1$.

The action is bounded by the topological charge as $S \geq \frac{8\pi^2}{g^2} |Q|$. Then, the instanton and the anti-instanton configurations are characterized by the (anti-)self-

duality condition,

$$G^a = \tilde{G}^a ; \quad (3)$$

which provides the action $S = \frac{8}{g^2} \int Q \cdot j$. These instanton solutions satisfy the general Yang-Mills field equations automatically, $D \cdot G = D \cdot \tilde{G} = 0$. The $Q = 1$ self-dual solution in the singular gauge is written as

$$A^I(x; z; \theta; 0) = \frac{a}{2} \frac{2iO^{ab} b (x - z)^2}{(x - z)^2 f(x - z)^2 + g^2}; \quad (4)$$

where a and z denote the size and the central coordinate of the instanton, respectively. The instanton solution can be rotated in color space by the color orientation matrix O . The 't Hooft symbol $_{ab}^{(b)}$ is defined as

$$_{ab}^{(b)} = \begin{cases} "b & ; & ; = 1; 2; 3 \\ b & ; & = 4: \end{cases} \quad (5)$$

On the other hand, we can obtain the anti-self-dual solution A^I by replacing $_{ab}^{(b)}$ to $_{ab}^{(b)} = (-1)^{a+1} \delta_{ab}$. The instanton solutions have several collective modes relating to the size and the position of instanton, which are described by one and four parameters, respectively. For pure SU(2) gauge theory, the color orientation matrix is characterized by 3 parameters as the Euler angle.

The instanton properties are investigated numerically by using a cooling procedure of the lattice QCD, which is achieved by an artificial reduction of the local lattice action. This method allows one to eliminate short-range quantum fluctuations of gluon fields and to extract excitations like instantons effectively from the nonperturbative QCD vacuum [20, 21]. The instanton properties, e.g. the instanton size distribution and the topological susceptibility, are estimated in the cooled gauge configuration dominated by instantons and anti-instantons.

We discuss now the appearance of the QCD monopole by taking the abelian gauge. The abelian gauge is defined by the diagonalization of a suitable gauge-dependent variable, $X(x) \in \text{su}(N_c)$. In this gauge, a nonabelian gauge theory as

QCD is reduced to an abelian gauge theory, and QCD monopoles appear from hedgehog configurations of $X(x)$. In order to understand the abelian gauge fixing and the appearance of monopoles, we consider a gauge function $\alpha(x) = e^{i^a(x)T^a} 2 \text{ SU}(N_c)$, which diagonalizes the gauge-dependent variable $X(x)$ as

$$X(x) \circ X(x) = \begin{pmatrix} 0 & X(x) & X(x) & \cdots & 0 \\ & 1 & & & \\ & & 1 & & \\ & & & \ddots & \\ & & & & 1 \end{pmatrix} \quad (6)$$

$$= \begin{pmatrix} 0 & & & & \\ & \ddots & & & \\ & & \ddots & & \\ & & & \ddots & \\ & & & & 0 \end{pmatrix} \begin{pmatrix} X_0(x) & & & & \\ & \ddots & & & \\ & & X_d(x) & & \\ & & & \ddots & \\ & & & & X_{N_c}(x) \end{pmatrix} \quad (7)$$

Here, $\lambda_i(x)$ is the i -th eigenvalue of $X(x)$, which depends on the space-time coordinate.

By such a gauge transformation $\alpha(x)$, the gauge field transforms as

$$A(x) \circ A(x) = \alpha(x) (A(x) + \partial_\mu \alpha(x)) \circ \quad (8)$$

In general, there remains the abelian gauge symmetry $U(1)^{N_c-1} \subset \text{SU}(N_c)$. However, the abelian gauge fixing can not be made on the point x_s which satisfies the degeneracy condition of the eigenvalue of $X(x)$, $\lambda_i(x_s) = \lambda_{i+1}(x_s)$. Such a degeneracy point x_s provides a monopole in the abelian sector.

We consider a pure $\text{SU}(2)$ gauge theory in order to investigate the appearance of monopoles at degeneracy points of the gauge-dependent variable, $X(x) = X^a(x) \frac{\sigma^a}{2}$. Here, the two eigenvalues can be given by $\lambda(x) = \frac{1}{2} \sqrt{X_1^2(x) + X_2^2(x) + X_3^2(x)}$. The degeneracy condition, $\lambda_+(x_s) = \lambda_-(x_s)$ can be obtained as $X^1(x_s) = X^2(x_s) = X^3(x_s) = 0$. Therefore, the degeneracy point forms point-like manifold on \mathbb{R}^3 , or line-like manifold on \mathbb{R}^4 . By using the Taylor expansion around the degeneracy point x_s , the variable $X(x)$ is generally written as

$$X(x) \approx \frac{1}{2} C^{ai} (x - x_s)^i + \# (x - x_s)^2; \quad (9)$$

where $C^{ai} = \frac{1}{2} X^a(x_s)$. We introduce new coordinates, $w^a = \text{sgn}(\det C) C^{ai} (x - x_s)^i$.

The variable X near the degeneracy point behaves as a hedgehog configuration,

$$X(w) = \frac{1}{2} w^a; \quad (10)$$

which is a mapping $w \in \mathbb{R}^3$ to $X(w) \in su(2)$ corresponding to $\begin{pmatrix} 1 & 0 \\ 0 & 1 \end{pmatrix} (SU(2) \times U(1)) = U(1)$. The topological feature does not change by this linear transformation from x_i to w_a around the degeneracy point.

By using the polar coordinates $w = (r\cos' \sin', r\sin' \sin', r\cos')$, we find a gauge function

$$(w) = \frac{1}{2} \begin{pmatrix} e^{i'} \cos_2 & \sin_2 \\ \sin_2 & e^{-i'} \cos_2 \end{pmatrix}; \quad (11)$$

diagonalizes the hedgehog configuration (10). After the gauge transformation, gauge fields are decomposed into two parts, $A(x) = A^{\text{reg}}(x) + A^{\text{sing}}(x)$, with the regular part $A^{\text{reg}}(x) = A(x) - A^{\text{reg}}(x)$ and the singular part $A^{\text{sing}}(x) = A(x) - A^{\text{reg}}(x)$. Since the multi-valuedness of the singular part happens at $\theta = 0$, there appears a singularity corresponding to the Dirac string on the positive side of the z -axis. To see this, we consider the abelian magnetic flux, $\langle \phi \rangle = \frac{1}{ie} \int_C^H dx \cdot A^{\text{sing}}$, which penetrates the area inside the closed contour C . At the pole $\theta = 0$, where the contour C shrinks into a point, the flux value is finite, $\langle \phi \rangle(0) = \frac{4}{e} \frac{\pi^2}{2} \neq 0$, which means the existence of the Dirac string. At another pole $\theta = \pi$, a trivial result, $\langle \phi \rangle(\pi) = 0$, is obtained. These results indicate that a monopole appears as a terminal point of the Dirac string. For hedgehog configurations of the gauge dependent variable X , there appear magnetic monopoles with the magnetic charge $g = \frac{4}{e}$ satisfying the Dirac condition.

In terms of the mathematical aspects of the gauge field, the monopole current k appears due to the singularity of the gauge transformation. In general, the field strength is defined as

$$G = \hat{D}^\mu \hat{D}_\mu - \hat{D}_\mu \hat{D}^\mu; \quad (12)$$

which returns to the standard definition $G = \hat{D}^\mu \hat{D}_\mu - \hat{D}_\mu \hat{D}^\mu = \partial_\mu A^\mu + A^\mu \partial_\mu$ for the regular case. Under the abelian gauge transformation (x) , the field strength

transform s as

$$G = G^Y = @ A @ A + [A; A] @; @]^Y; \quad (13)$$

Since the last term is diagonal, abelian field strength is naturally obtained as

$$F = @ a @ a @; @]^Y; \quad (14)$$

by performing the abelian projection, $A^{\text{AP}} = A - \text{tr}(A^3) \frac{3}{2}$. The abelian Bianchi identity is broken due to the existence of the last term in Eq.(14), and the magnetic current $k(x)$ is obtained as

$$k(x) = \frac{1}{2} @ F \quad (15)$$

$$= \frac{1}{2} @ [@; @]^Y; \quad (16)$$

The obvious consequence of the monopole current conservation, $\partial k = 0$, means that monopole currents form closed loops.

3 Correlation between Instanton and Monopole for Color Connection

Recently, both analytical and lattice studies found a strong correlation between instantons and monopoles in the abelian projected theory of QCD [27]–[38].

It is easy to prove that monopoles appear around instanton centers by taking the Polyakov-like gauge, where $A_4(x)$ is chosen as the gauge-dependent variable $x(x)$ [27]. The fourth component of the instanton configuration has a hedgehog configuration around the center z_k of the k -th instanton,

$$A_4^I(x) = i_k^2 \frac{^a(x - z_k)^a}{(x - z_k)^2 f(x - z_k)^2 + g_k^2}; \quad (17)$$

The appearance of monopoles is caused by the existence of the hedgehog configurations near instanton centers in the Polyakov-like gauge. We can find that $A_4(x)$ is diagonalized by the gauge function, $x = e^{i_3} \cos \frac{x}{2} + i(\cos \frac{x_1}{2} \sin \frac{x_2}{2} + \sin \frac{x_1}{2} \cos \frac{x_2}{2})$, where α and

are the parameters of spherical coordinates from the instanton center, and θ is an arbitrary constant. This gauge function $\chi(x)$ can be taken as t -independent,

$$\begin{aligned} X(x) = A_4(x) + X(x) &= (\chi) (A_4(x) + \theta_4)^{-1}(x) \\ &= (\chi) A_4(x)^{-1}(x) = A_4^d(x); \end{aligned} \quad (18)$$

The gauge field is transformed as $A(x) = (\chi) (A(x) + \theta)^{-1}(x)$, and this second term includes singularity $A^{\text{sing}}(z_k) = (\chi) \theta^{-1}(x) \frac{1}{z_k}$ at the hedgehog center of $X(x)$. Therefore, the monopole world-line penetrates the center of the instanton, $x = (z_1; t)$, ($-1 < t < 1$), on the 4-dimensional space-time.

In the MA gauge, on the other hand, the correlation between instantons and monopoles is investigated both in analytical and lattice studies [32, 35]. The MA gauge is obtained by minimizing the functional R_{ch}

$$R_{\text{ch}}[A] = \int d^4x f(A^1(x))^2 + (A^2(x))^2 g; \quad (19)$$

which means that off-diagonal part of gluon fields is minimized by the gauge transformation. Thus, this gauge fixing should result in the dominance of diagonal part. The stationary point of $R_{\text{ch}}[A]$ is provided by the derivative condition,

$$(\theta - A^3)A = 0; \quad A = A^1 - iA^2; \quad (20)$$

It is noted that self-dual solutions like instantons satisfy the stationarity condition (20) automatically, which leads the appearance of monopole currents near each instanton. This stationarity condition is not sufficient to realize the MA gauge and actually, the functional $R_{\text{ch}}[A]$ must be minimized. A single instanton configuration gives a finite value $R_{\text{ch}}[A^s] = 4^{-2}$ with R being the instanton size in the singular gauge, which has a point singularity at the instanton center. For the instanton solution in the nonsingular gauge, there appears the divergence as $R_{\text{ch}}[A] = 2^R d^4x \frac{2}{(x^2 + R^2)^2} \neq 1$.

By a comparison between the singular and the nonsingular gauge, Brower et al. found that the intermediate gauge satisfies also the local MA conditions (20), which leads a monopole loop of radius R centered around an instanton [35]. The monopole loop radius R should be decided by minimizing the functional $R_{ch}[\mathbf{A}]$. In the single instanton case, the monopole loop with radius R prefers to shrink to a point. This fact is natural from the following consideration. There is no definite direction of the single instanton due to the 4-dimensional rotation invariance. Therefore, the normal vector of the monopole loop can not be fixed and the loop ought to shrink to a point as the volume goes to the infinite. However, the R dependence of $R_{ch}[\mathbf{A}]$ is found to be extremely small. It is investigated on the lattice by Hart and Teper [32] that a single instanton produces a closed monopole loop with a finite radius corresponding to the instanton size. Some small perturbation as the presence of the finite volume and the finite lattice size may cause these results due to the fragile nature of the monopole point solution. Actually, there are many pairs of separated instanton and anti-instanton in the QCD vacuum. Then, monopole loops appear independently around each center of the instanton and the anti-instanton due to the small perturbation on each other. As the distance among them gets short, the individual monopole loops are combined into a longer stable loop by hopping from one instanton to the other.

The QCD vacuum possesses the gluon condensate [40], which relates to the number of instantons and anti-instantons. If the total action can be estimated as the sum of individual instanton actions, the gluon condensate is proportional to the instanton density as $\frac{1}{32\pi^2}hG^a G^a i' (N = V)$. The QCD sum rule provides the phenomenological value $\frac{1}{32\pi^2}hG^a G^a i' (200 \text{ MeV})^4$ and then, the average instanton density $(N = V) \approx 1 \text{ fm}^{-4} = (200 \text{ MeV})^4$ by the above assumption. The average instanton size is obtained from instanton liquid models and lattice calculation, $\approx (0.33 - 0.4) \text{ fm}$ [41]. These scale parameters suggest that the QCD vacuum is the dense matter of

instantons and anti-instantons overlapping each other.

On the other hand, the large monopole clustering is observed in the confinement phase by using lattice QCD simulations. The very long and highly complicated monopole trajectory is identified as a signal of monopole condensation being responsible for confinement. As the temperature increases, the nonperturbative nature of the QCD vacuum changes drastically into the perturbative one at the critical temperature. At high temperature, such a long monopole loop disappears and there remain only short monopole loops.

In addition to these vacuum structures, the strong correlation between instantons and monopoles in the MA gauge motivates us to study monopole clustering and color confinement in terms of instantons. We would like to investigate the origin of the promotion of long monopole loops by using a more realistic multi-instanton system on the R^4 space. If this is the case, the instanton is expected to play a relevant role on the confinement mechanism via the promotion of long monopole loops. In order to clarify the relation of instantons with color confinement, we calculate the static quark potential in the multi-instanton system by using the Wilson loop. We concentrate on the instanton density, which may change drastically at the confinement-deconfinement phase transition of the finite temperature QCD, and would like to discuss the structure of the QCD vacuum in terms of instantons.

4 Multi-Instanton Model

In this section, we would like to model the nonperturbative QCD vacuum in terms of instantons. As the lattice QCD simulations suggest, the QCD vacuum is filled with many instantons and anti-instantons, and therefore it is to be modeled by the multi-instanton ensemble. First of all, we consider the partition function Z_{inst}^1 of the single

instanton as the basic ingredient of the multi-instanton theory. Using the collective coordinates, z, θ, ϕ , the single partition function is expressed as

$$Z_{\text{inst}}^1 = \int d^4z \int d\theta d\phi f_0(z); \quad (21)$$

$$f_0(z) = \frac{C(N_c)}{5} \left[\frac{8^2}{g^2(M)} \right]^{2N_c} (M)^b \exp\left(-\frac{8^2}{g^2(M)}\right) \quad (22)$$

with $b = \frac{11}{3}N_c$. Here, $f_0(z)$ is the single instanton weight function in the one-loop approximation [42, 43]. This weight function has a scale M corresponding to the scale invariance breaking by the trace anomaly in QCD. The weight function $f_0(z)$ with $N_c = 2$ increases with the instanton size z , and the infrared divergence appears in Z_{inst}^1 within the one-loop approximation, which is discussed in the multi-instanton system.

We consider now the multi-instanton system as an ensemble of single instantons. The multi-instanton partition function is given by

$$Z \sim \frac{1}{N_+ N_-} \frac{1}{N_+! N_-!} \prod_{n=1}^{N_+ + N_-} \int d^4z_n \int d\theta_n d\phi_n f_0(z_n) \exp(-U_{\text{int}}(z_n; \theta_n; \phi_n)) g; \quad (23)$$

Here, U_{int} is the interaction between instantons (anti-instantons) and generally depends on z_n, θ_n, ϕ_n . However, we follow the standard method, where the interaction is taken to depend only on the size z [44, 45, 46]. Therefore, we consider now the instanton size distribution $f(z) = f_0(z) \exp(-U_{\text{int}}z)$. This interaction is found to be repulsive, which suppresses the appearance of large size instantons [44, 45, 46]. We regard the positions and the color orientations as random variables in our calculation.

For the small instanton, the perturbative scheme is valid and the interaction U_{int} can be neglected. Hence, the instanton size distribution $f(z)$ behaves as $f_0(z)$,

$$f(z) \sim \text{const}^{-b/5}; \quad (24)$$

On the other hand, for the large instanton, the direct estimation of $f(z)$ is very complicated due to the nonperturbative properties. However, the analytical studies and

the numerical lattice calculations [47, 48] suggest a strong suppression of the large size instanton in the infrared region as

$$f(\rho) \stackrel{\rho \rightarrow 0}{\sim} \text{const} \quad ; \quad (25)$$

which is caused by the infrared repulsive force. The ordinary instanton liquid model suggests $\beta = 5$ [48]. Furthermore, we try to calculate another typical case with $\beta = 3$, where a linear component potential is reproduced [47]. In this case, instantons overlap each other and here, we may not have a simple form like the sum ansatz for the multi-instanton ensemble's construction. However, the infrared behavior of the size distribution in the QCD vacuum is not known until now. In our calculation, we take $\beta = 5$ and 3 for the size distribution on large instantons.

In order to connect the two distributions smoothly, we take the size distribution as

$$f(\rho) = \frac{1}{(\frac{\rho}{\rho_1})^3 + (\frac{\rho}{\rho_2})^{3\beta/5}} \quad (26)$$

where ρ_1 denotes the infrared size parameter and ρ_2 the ultraviolet size parameter. There two parameter is fixed by the average instanton size $\langle \rho \rangle = 0.4 \text{ fm}$ [41] and the normalization condition.

The above discussion amounts to use the partition function instead of (23)

$$Z \sim \prod_{n=1}^{N+Y} \int d^4 z_n \frac{Z_n}{d_n} \frac{Z_n}{d\Omega_n} \frac{1}{(\frac{\rho}{\rho_1})^3 + (\frac{\rho}{\rho_2})^{3\beta/5}} \quad (27)$$

As for the gluon field A^I of the multi-instanton system, we take the sum ansatz [49],

$$A^I(\mathbf{x}) = \sum_k^X A^I(\mathbf{x}; z_k; \mathbf{z}_k; \Omega_k) + \sum_k^X A^I(\mathbf{x}; z_k; \mathbf{z}_k; \Omega_k); \quad (28)$$

which is constructed by the instanton and anti-instanton solutions in the singular gauge. By using this ansatz, D' Iakonov and Petrov have suggested in the variational treatment that there appears some repulsive force at infrared region.

In actual calculations, we generate the ensemble of instantons and anti-instantons with random centers z_k on the 4-dimensional Euclidean continuum space. The color orientations O_k are taken randomly. The instanton sizes r_k are randomly chosen following the size distribution $f(r)$ in Eq.(26). In our model construction, the interaction among these pseudoparticles is supposed to be included effectively in the instanton size distribution $f(r)$ in the simple sum ansatz.

5 Monopole Clustering in Multi-Instanton System

We investigate the monopole-loop distribution in the multi-instanton system after the maximally abelian (MA) gauge fixing [37, 38]. We use a 32^4 lattice with the lattice-spacing, $a = 0.125$ fm, which means the total volume, $V = (4.0 \text{ fm})^4$. For each case $\bar{r} = 3; 5$, the average instanton size is fixed as $\bar{r} = \sqrt[3]{d} \int f(r) r^2 dr = 0.4 \text{ fm}$. The instanton size distribution for $\bar{r} = 3$ and 5 are shown in Fig.1. First of all, we discuss here the boundary condition of an instanton ensemble on the 4-dimensional space with the finite volume L^4 . We assume that instantons appear periodically with the period of the size. A schematic view of this periodic condition of an instanton ensemble sliced into 2-dimensional plane is shown in Fig.2. We then calculate the gluon field of one finite volume by calculating the contributions of all the instantons in the neighboring boxes including the ones of the box of interest. This means the consideration of the instantons in the 3^4 boxes in the 4-dimensional case: it is $3^2 = 9$ boxes in the 2-dimensional case as shown in Fig.2. This procedure establishes a sufficient strength of the gluon field near the box boundary.

Now, we introduce a lattice on the multi-instanton configuration and define the link variable, $U(s) = \exp(i\alpha A(s))$, where $A(s)$ is provided on each site from Eq.(28). We calculate the link variable by considering all the instantons in the neighboring boxes.

We apply the MA gauge fixing [6], which maximizes

$$\begin{aligned}
R &= \sum_{s=0}^X \text{tr}[U(s)^3 U^Y(s)^3] \\
&= 2 \sum_{s=0}^X [(U^0(s))^2 + (U^3(s))^2 - (U^1(s))^2 - (U^2(s))^2] \\
&= 2 \sum_{s=0}^X [1 - 2f(U^1(s))^2 + (U^2(s))^2 g];
\end{aligned} \tag{29}$$

here $U(s) = U^0(s) + i^i U^i(s)$. The maximization of R corresponds to the lattice expression of the minimizing condition of $R_{ch}[A]$ in Eq.(19). In the MA gauge, SU(2) link variable $U(s)$ are decomposed as

$$\begin{aligned}
U(s) &= \frac{M_0(s)u(s)}{1 - jc(s)} \\
&= \frac{e}{c(s)} \frac{c(s)}{1 - jc(s)} \begin{pmatrix} 1 & e^{i(s)} & 0 \\ 0 & e^{-i(s)} & 0 \end{pmatrix};
\end{aligned} \tag{30}$$

where the abelian angle variable $i(s)$ and $c(s)$ are related with $U(s)$ as

$$\tan(i(s)) = \frac{U^3(s)}{U^0(s)} \tag{31}$$

$$c(s) = [U^2(s) + iU^1(s)]e^{-i(s)}: \tag{32}$$

It is obvious from the expression of Eq.(29) that the off-diagonal part $U^1(s)$ and $U^2(s)$ of gluon fields is minimized by the MA gauge transformation. Therefore, full SU(2) link variables would be approximated as $U(1)$ link variables, $U(s) \approx u(s)$.

The monopole current can be defined by using $u(s)$ following DeGrand and Toussaint [50]. By using a forward derivative $\partial f(s) = f(s+\Delta) - f(s)$ with unit vector $\hat{\Delta}$, the 2-form of the lattice formulation, $\epsilon(s) = \partial(s) \wedge \partial(s)$, is decomposed as

$$\epsilon(s) = \epsilon(s) + 2n(s) \tag{33}$$

with $\epsilon(s) \in \text{mod}_2$ and $n(s) \in \mathbb{Z}$. Here, $\epsilon(s)$ and $2n(s)$ correspond to the regular part and the singular Dirac string part, respectively. Since the Bianchi identity regarding the abelian field strength $\epsilon(s)$ is broken, the monopole

current $k(s)$ can be defined on the dual site s as

$$k(s) = \frac{1}{4} n(s+^) = \partial n(s) \quad (34)$$

where $n(s) = \frac{1}{2} n(s+^)$. The obvious current conservation law $\partial^0 k(s) = 0$ leads to the closed monopole loop in the 4-dimensional space. Here, ∂^0 denotes a backward derivative. With the above procedure, we measure the monopole-loop length for various multi-instanton configurations.

Furthermore, we execute also a "block-spin" transformation on the dual lattice with the scale factor N . The spike appearing at small monopole-loop length is due to the numerical noise in the short distance and disappears by the "block-spin" transformation in order to emphasize the large distance physics. Here, the N^3 extended monopole is defined as

$$n^N(s) = \sum_{i,j=0}^{N-1} n(ns + i^+ + j^+) \quad (35)$$

on a sublattice with the spacing $b = N a$ [51]. Then, we consider the extended monopole current, $k^N(s) = \frac{1}{2} n^N(s+^)$, in order to investigate the global networks of monopole currents, which may be identified as the signal of monopole condensation.

In order to clarify the local correlation between instantons and monopoles, we start with a very dilute instanton density ($N = V$) $(0.5 \text{ fm})^4 = (100 \text{ MeV})^4$, where instantons are separated completely from each other. In this situation we expect that a monopole loop prefers to shrink to a instanton center. However, on the lattice, we observe each finite monopole loop is localized around each instanton center as shown in Fig.3-a. Such a small monopole loop is caused by finite lattice volume and lattice spacing and is numerically washed out by several numbers of "block-spin" transformation.

In the QCD vacuum, on the other hand, instantons distribute in the 4-dimensional

space close to each other with a instanton density of $N = V = (1/fm)^4$ [1] and overlap among each other somewhat even with the repulsive interaction among them. These interaction is known to be repulsive between instanton and anti-instanton, which suppress the large size instanton. We shall take into account the repulsive interactions effectively by introducing the instanton size distribution $f(\cdot)$, which decreases rapidly with increasing the size \cdot , instead of the actual interaction and generate the instanton ensemble with such a size distribution.

We investigate typical instanton density cases, $(N = V)^{1/4} = 0.5, 1.0$ and $1.5 = fm$, for each extended monopole loop. Fig.4-a denotes the histogram of the unblocked monopole loop. Fig.4-b, 4-c and 4-d denote the cases of the monopole loops on the sublattice with $b = 2a$, $b = 4a$ and $b = 8a$, respectively. Also, we show the histograms corresponding to $\cdot = 3$ in Fig.5. At low instanton density, relatively short monopole loops appear only around isolated instantons as shown in Fig.3-a. This situation provides a the peak at zero monopole length in the histogram of monopole-loop lengths as Fig.4-b.

As the density increases, some monopole trajectory tends to hop from one instanton to another nearby instanton as shown in Fig.3 and as a result, there appear long monopole loops. In the histogram, a clustering of the long monopole loops appears and grows gradually to be separated from the small monopole loop part. Here, the "block-spin" transformation clearly removes small size monopole loops and besides, combine several long monopole loops into one. This procedure is available to clarify monopole loop behaviors from the long-range view point, as can be seen in Fig.8, 4-a, 4-b and 4-c. At high instanton density, there appears one very long and highly complicated monopole loop in each gauge configuration as shown in Fig.4-b. The appearance of the monopole clustering over the entire physical volume can be interpreted as the

Kosterlitz-Thouless-type phase transition [52]. It is noted that this system is constructed by smooth configurations like instantons. If short range quantum fluctuations $a(x)$ around classical instanton configurations is considered, $A(x) = A^I(x) + a(x)$, we expect the appearance of more complicated and longer monopole loops.

We compare the results with those of the true SU(2) lattice QCD with $16^3 \times 4$ at different temperatures ($\beta = 2.2$ and 2.35) in Fig.7 [36]. The monopole-loop distribution at the high instanton density case resembles that in the confinement phase ($\beta = 2.2$). On the other hand, the dilute instanton system is similar to the deconfinement phase obtained by the lattice QCD ($\beta = 2.35$) on the viewpoint of the large monopole disappearance. Such resemblance seems to indicate an important role of instantons on confinement in the QCD vacuum. At low temperature where monopole condensation is realized, many instantons exist while overlapping each other with the instanton density $(N = V)^{1/4}$ and may characterize the nonperturbative feature of QCD vacuum. As the temperature increases, the instanton density is largely reduced as suggested in the lattice QCD simulation. In this situation, each instanton becomes isolated, and the monopole loop originating from the instanton tends to be localized around each instanton. Above the critical temperature which the color confinement is not realized, these pseudoparticles almost disappear and, as a result, there remain only small monopole loops. These results indicate that instantons are relevant degrees of freedom for the promotion of large monopole loops. Furthermore, drastic changes of the instanton density at finite temperature may cause two typical distributions of the monopole-loop length, which characterize the confinement and the deconfinement phase through monopole condensation.

6 Color Connection in Multi-Instanton System

In the previous section, we have discussed that the high-density instanton system provides highly complicated monopole loops. We further work out the connecting property without referring to monopole configurations in the abelian gauge. To this end, the consideration of the Wilson loop with the contour C is useful for the investigation of connection properties directly for the multi-instanton system [53].

$$W[C] = \text{tr}^P \exp [i \int_C A^I dx^I] = \text{tr}^Y U(s); \quad (36)$$

If the contour C is a rectangle of dimension T by R , the Wilson loop is related to the static quark potential as $V(R) = \lim_{T \rightarrow 1} f \ln W(R; T) = T g$. When one uses this relation to extract the potential without the contamination of excited states, T has to be large enough compared to the distance R between quarks, $T \gg R$ [58].

Hence, we want to take a large enough time T in the lattice simulations. However, when we use the periodic conditions, which were necessary to extract the color monopole currents as discussed in the previous section, we are limited to the time distance as a half of $N_t a$, where N_t is the number of lattice in the time direction and a is the lattice unit. Therefore, we introduce a 36^4 lattice only in the center of the 4-dimensional instanton configurations, whose total volume is fixed to be $V = (10 \text{ fm})^4$, without the periodic condition for the sizes, positions and color orientations of instantons as shown in Fig. 8. In order to calculate the large Wilson loop, we can take in this case T equal to the lattice size $L' = 36 a$. We consider the instanton ensemble with the number $N = N_+ + N_- = 10^4$ in the volume $(10 \text{ fm})^4$ corresponding to the instanton density $(N/V) = (10 \text{ fm})^4$. In this case, we need a fine lattice of the unit $a = 0.05 \text{ fm}$ in order to justify the continuity of the link variables, which are the exponentials of the summation of instantons and anti-instantons, $U(s) = \exp [ia \sum_{N_+, N_-}^P (\tilde{A}_I + \tilde{A}_{\bar{I}})]$.

We have to then the multi-instanton configurations. For this, we take the recent lattice studies, which provide instanton properties, the averaged instanton size, the instanton density ($N = V$). In order to extract the instanton configurations we have to smooth out the smoothed QCD vacuum by using several cooling methods. DeGrand et. al. investigate a smoothing procedure based on the renormalization group equation [54]. In this $SU(2)_c$ lattice calculation, the average size of instantons is found to be about $\langle r \rangle = 0.2 \text{ fm}$ at a density of about $(N = V) = 2 \text{ fm}^{-4}$. On the other hand, de Forcrand et. al. use a cooling algorithm based on an improved action with scale invariant instanton solution and provide that the instanton size distribution is peaked around 0.43 fm with a susceptibility of about $\chi = (200 \text{ MeV})^4$ [55]. These two cooling methods provide different values about the averaged instanton size. As for the instanton size distribution, there are many efforts to extract a size distribution from the lattice configurations by various smoothing methods [54, 55, 56]. However, there is no consensus on the size distribution either. In our calculation, we take the instanton density as $(N = V) = (1 = \text{fm})^4$ and the averaged instanton size 0.4 fm . These values are used in the discussion of the chiral symmetry breaking [57]. Furthermore, with these parameters we get the monopole length distribution in the range of those obtained by QCD simulation as discussed in the previous section [38]. We consider the total topological charge is zero, which means the equal numbers of instantons and anti-instantons; $N_I = N_{\bar{I}} = N = 2$. As used for the study of monopoles, we take the fall-off parameters of the instanton size distribution as $\alpha = 3$ and 5 .

We perform 36^4 lattice simulations with the instanton configuration as discussed above. We show the calculated results in Fig.9 on the Wilson loop for the case of $\alpha = 5$. The Wilson loop obeys the area law, which indicates the existence of the linear confining potential. In such a situation that the Wilson loop decays as $\exp[-R/T]$, the errors of this value grow as the area R/T increases since the Wilson

loop decreases exponentially with R/T . One way to reduce the errors is the smearing procedure which replaces the usual link variable $U(s)$ to a smeared link variable, $\bar{U}(s) = cU(s) + \frac{P}{\epsilon} U(s)U(s+\epsilon)U^Y(s+\epsilon)$, with normalization constant c in order to smooth out the ultraviolet noise. However, in our calculation we estimate the expectation value of Wilson loops constructed by the original link variable $U(s)$ on 500 complete independent configurations on the 36^4 lattice. Using such a large lattice we can calculate as much as 10^4 measurements of Wilson loops, which are assumed to be statistically independent, on each instanton configuration. Fig.10 shows that the static quark potential $V(R)$, which is proportional to the inter-quark distance R up to the intermediate region $R' \approx 1.2\text{ fm} < T$. We checked that the static potential in this region $R' \approx 1.2\text{ fm}$ does not depend on T within errors. Also, we show the results for $\beta = 3$ in Fig.11 and 12, respectively. The results are qualitatively very similar.

If we want to discuss the behavior of Wilson loop at longer range region $R > 1.2\text{ fm}$, the Wilson loop must be calculated at large $T = 2.0\text{ fm}$, which means a calculation for the smaller value of Wilson loops $W[R;T]/\exp[-RT]$. In order to estimate the expectation value of Wilson loops at larger R, T and also with large string tension, we need a huge number of the independent measurements and perform the smearing procedure in order to reduce the statistical error.

Furthermore, we discuss the relation between the strength of color content and the instanton density. We take three cases with $(N = V)^{\frac{1}{4}} = 0.50, 0.75$ and $1.00 = \text{fm}$. In order to extract the string tension, we shall measure the Creutz ratio

$$\frac{hW(R;T)i hW(R-1;T-1)i}{hW(R;T-1)i hW(R-1;T)i} \quad (37)$$

from the SU(2) Wilson loop. If the logarithm of the Wilson loop can be approximated as $\ln W(R;T)i = -RT + m(R+T) + \text{const}$, the Creutz ratio gives the exponent of the string tension, $\gamma = \exp(-\frac{1}{\text{lat}})$. The dimensionless lattice string tension lat

provides the physical string tension τ_{phys} with the lattice unit a as $\tau_{\text{phys}} = \tau_{\text{lat}} = a^2$.

We show the string tensions around $R = 0.8\text{ fm}$ as a function of the instanton density in Fig. 13 and 14 corresponding to $\tau = 5$ and $\tau = 3$ cases, respectively. At a density of $(N = V) = (1\text{ fm})^4$ with $\tau = 5$, the string tension comes out to be about 0.4 GeV fm , corresponding to $2/5$ of the physical string tension. Brower et. al. suggests that at the density $(N = V) = (1\text{ fm})^4$ of the instanton liquid model the slope of the heavy quark potential is about 0.1 GeV fm [59]. These different may be caused by the different choice of the averaged instanton size. The string tension depends not only on the averaged instanton size but also on the instanton density directly. The string tension reduces drastically as the instanton density decreases. This tendency seems to indicate the disappearance of the string tension as the decreasing number of instantons and anti-instantons, which is suggested by the finite temperature lattice QCD.

7 Conclusion

We have studied color component and nonperturbative quantities of the QCD vacuum using the multi-instanton configuration. We have made the present study by being motivated by the presence of a strong correlation between instantons and monopoles after the abelian gauge fixing in pure $SU(2)$ gauge theory. We believe that this correlation leads to a new approach for the color component mechanism through monopole clustering in terms of instantons. In our calculation, the multi-instanton system is constructed by assuming the suppression of the large size instanton by due to the infrared repulsive interaction between instantons and anti-instantons.

First, we have investigated the monopole-loop distribution in the multi-instanton system by using the maximally abelian gauge. The dilute instanton density system

produces short and simple monopole trajectories. A small monopole loop is localized around each instanton, which is isolated from other instantons. If instantons are too far from each other, monopole loops disappear as the continuum limit $\lambda \rightarrow 0$. However, as the instanton density becomes higher, several small monopole loops combine into one very long and highly complicated monopole loop, which covers the entire physical vacuum. The appearance of long monopole loops of this system resembles that of low temperature lattice QCD which realizes color confinement through monopole condensation.

We have found that the high instanton density provides a highly complicated and long monopole loop. This seems to indicate that the instantons are responsible also for confinement. Therefore, we have calculated the static quark potential in the multi-instanton system directly. Here, the Wilson loop is a useful measure for the confinement properties without executing the abelian gauge fixing. We have found that the instanton ensemble gives the area law behavior of the Wilson loop and the static quark potential is approximately proportional to the inter-quark distance, $V(R) \propto R$, up to $R \leq 1.2 \text{ fm}$. The string tension takes the experimental value $\sigma = 0.4 \text{ GeV fm}$ for the probable instanton density ($N = V$) = $(1 \text{ fm})^4$ and average instanton size $\langle R \rangle = 0.4 \text{ fm}$ with $N = 5$. The string tension tends to decrease monotonously as the instanton density becomes smaller. Such a tendency is consistent with the disappearance of long monopole loop as the instanton number is reduced. These instanton parameters, ($N = V$) and $\langle R \rangle$, can be calculated by using the lattice QCD based on several cooling procedures. However, this procedure not only reduces quantum fluctuations but also lead to instanton and anti-instanton pair annihilation and finally change the instanton properties. Therefore, different results are given by using several cooling methods based on different schemes, for instance inverse-blocking and improved cooling so on. The instanton density and the instanton size are not still known in the original QCD

vacuum, that is before the cooling.

The instanton seems to be a relevant degree of freedom for the promotion of long monopole loops. Besides, such a multi-instanton system provides a linear potential up to $R \approx 1.2\text{ fm}$. Although the string tension is about a half of that of the QCD vacuum, the instanton plays an important role for the linear potential among quarks in the physically interesting region. However, it is necessary to simulate the static quark potential at long distance ($R \approx 1.2\text{ fm}$) using larger Wilson loop and enormous configurations in order to clarify the constituent properties up to very long distance. This desire is facing with the limit of the present computation power.

8 Acknowledgment

We would like to thank Dr. S. Sasaki for his useful comments and discussions. We would like to thank Dr. A. Tanaka for his continuous encouragement. One of the authors (H. S.) is supported in part by Grant for Scientific Research (No. 09640359) from the Ministry of Education, Science and Culture, Japan. One of the authors (M. F.) is supported by Research Fellowships of the Japan Society for the Promotion of Science for Young Scientists. We have performed all numerical simulations in this paper on NEC SX 4 at RCNP.

References

- [1] T. Schäfer and E. Shuryak, *Rev. Mod. Phys.* 70 (1998) 323.
- [2] G. 't Hooft, *Nucl. Phys.* B 190 (1981) 455.
- [3] Y. Nambu, *Phys. Rev.* D 10 (1974) 4262.
- [4] G. 't Hooft, in *High Energy Physics* (Editorice Compositori, Bologna, 1975).
- [5] S. Mandelstam, *Phys. Rep.* C 23 (1976) 245.
- [6] A. Kronfeld, G. Schierholz and U.-J. Wiese, *Nucl. Phys.* B 293 (1987) 461.

[7] A. K. Ronfeld, M. Laursen, G. Schierholz and U.-J. Wiese, Phys. Lett. B 198 (1987) 516.

[8] F. Brandstater, U.-J. Wiese and G. Schierholz Phys. Lett. B 272 (1991) 319.

[9] S. Hioki, S. Kitahara, S. Kiura, Y. Matsubara, O. Miyamura, S. Ohno and T. Suzuki, Phys. Lett. B 272 (1991) 326.

[10] S. Kitahara, Y. Matsubara and T. Suzuki Prog. Theor. Phys. 93 (1995) 1.

[11] O. Miyamura, Phys. Lett. B 353 (1995) 9; Nucl. Phys. B (Proc. Suppl.) 42 (1995) 538.

[12] R. Wobshyn, Phys. Rev. D 51 (1995) 6411.

[13] Z. F. Ezawa and A. Iwazaki, Phys. Rev. D 25 (1982) 2681; D 26 (1982) 631.

[14] T. Suzuki and I. Yotsuyanagi Phys. Rev. D 42 (1990) 4257

[15] H. Suganuma, S. Sasaki and H. Toki, Nucl. Phys. B 435 (1995) 207.

[16] S. Sasaki, H. Suganuma and H. Toki, Prog. Theor. Phys. 94 (1995) 733.

[17] S. Sasaki, H. Suganuma and H. Toki, Phys. Lett. B 387 (1996) 145.

[18] A. Belavin, A. Polyakov, A. Shvarts and Yu. Tyupkin, Phys. Lett. B 59 (1975) 85.

[19] R. Rajaraman, 'Solitons and Instantons' (North-Holland, Amsterdam, 1982) 1.

[20] M. Teper, Phys. Lett. B 162 (1985) 357.

[21] M. Polikarpov and A. Veselov, Nucl. Phys. B 297 (1988) 34.

[22] G. 't Hooft, Phys. Rev. Lett. 37 (1976) 8; Phys. Rev. D 14 (1976) 3432.

[23] E. Witten, Nucl. Phys. B 149 (1979) 285, Nucl. Phys. B 156 (1979) 269.

[24] G. Veneziano, Nucl. Phys. B 159 (1979) 213.

[25] E. Shuryak and J. Verbaarschot, Nucl. Phys. B 341 (1990) 1.

[26] A. Polyakov, Nucl. Phys. B 120 (1977) 429.

[27] H. Suganuma, K. Itakura, H. Toki and O. Miyamura, nonperturbative Approaches to QCD, (PNPI, 1995) 224.

[28] H. Suganuma, H. Ichie, S. Sasaki and H. Toki, Color Confinement and Hadrons, (World Scientific, 1995) 65.

[29] O. Miyamura and S. Origuchi, Color Confinement and Hadrons, (World Scientific, 1995) 235.

[30] S. Thuner, H. Markum and W. Sakuler, Color Confinement and Hadrons (World Scientific, 1995) 77.
H. Markum, W. Sakuler and S. Thuner, Nucl. Phys. B (Proc. Suppl.) 47 (1996) 254.

[31] M. Polikarpov, Nucl. Phys. B (Proc. Suppl.) 53 (1997) 134.

[32] A. Hart and M. Teper, Phys. Lett. B 371 (1996) 261.

[33] H . Suganuma, A . Tanaka, S . Sasaki and O . M . Iyamura, Nucl. Phys. B (Proc. Suppl.) 47 (1996) 302.

[34] V . Bomyakov and G . Schierholz, Phys. Lett. B 384 (1996) 190.

[35] R . Brower, K . O riginos and C . Tan, Phys. Rev. D 55 (1997) 6313.

[36] H . Suganuma, S . Sasaki, H . Ichie, H . Toki and F . Araki, Frontier '96 (World Scientific,1997) 177. H . Suganuma, S . Sasaki, H . Ichie, F . Araki and O . M . Iyamura Nucl. Phys. B (Proc. Suppl.) 53 (1997) 528.

[37] M . Fukushima, A . Tanaka, S . Sasaki, H . Suganuma, H . Toki and D . D iakovov, Nucl. Phys. B (Proc. Suppl.) 53 (1997) 494.

[38] M . Fukushima, S . Sasaki, H . Suganuma, A . Tanaka, H . Toki and D . D iakovov, Phys. Lett. B 399 (1997) 141.

[39] H . Suganuma, H . Ichie, A . Tanaka, K . Amemiya, YKIS '97 Non-Perturbative QCD : Structure of the QCD Vacuum hep-lat/9804027.

[40] M . Shifman, A . Vainshtein and V . Zakharov, Nucl. Phys. B 147 (1979) 385.

[41] E . Shuryak, Nucl. Phys. B 203 (1982) 93; ibid 116.

[42] G . 't Hooft, Phys. Rev. Lett. 37 (1976) 8.

[43] C . Bernard, Phys. Rev. D 19 (1979) 3013.

[44] D . D iakovov and V . Petrov, Phys. Rev. D 50 (1994) 266.

[45] E . Shuryak and J . Verbaarschot, Phys. Rev. D 52 (1995) 295.

[46] E . Shuryak, 'The QCD Vacuum , Hadron and The Superdense Matter' (World Scientific 1988) 1.

[47] D . D iakovov and V . Petrov, Non-perturbative Approaches to QCD (PNPI,1995) 239.

[48] E . Shuryak, Phys. Rev. D 52 (1995) 5370.

[49] D . D iakovov and V . Petrov, Nucl. Phys. B 245 (1984) 259.

[50] T . D eg rand and D . Toussaint, Phys. Rev. D 22 (1980) 2478.

[51] T . L . Ivanenko, A . V . Pochinskii and M . I . Polikarpov, Phys. Lett. B 252 (1990) 631.

[52] J . M . Kosterlitz and D . J . Thouless J . Phys. C 6 (1973) 1181.

[53] M . Fukushima, H . Suganuma, A . Tanaka, H . Toki and S . Sasaki, Nucl. Phys. B (Proc. Suppl.) 63A -C (1998) 513.

[54] T . D eg rand, A . Hasenfratz and T . Kovacs, Nucl. Phys. B 520 (1998) 301.

[55] P . de Forcrand, M . Perez, I . Stamatescu, Nucl. Phys. B 499 (1997) 409.

[56] C . M ichael and P . Spencer Phys. Rev. D 52 (1995) 4691.

[57] D . D iakovov and V . Petrov, Phys. Lett. 147B (1984) 351.

[58] D . D iakovov and V . Petrov, hep-lat/9810037.

[59] R . Brower, D . Chen, J . Negele, E . Shuryak, hep-lat/9809091.

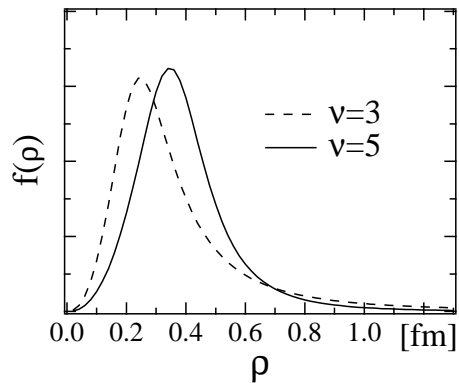


Figure 1: The instanton size distribution as a function of the instanton size ρ . The instanton size distribution for $\nu = 5$ is denoted by solid curve and that for $\nu = 3$ by dash curve. In both cases, the average size $\langle \rho \rangle$ is kept $= 0.4$ fm.

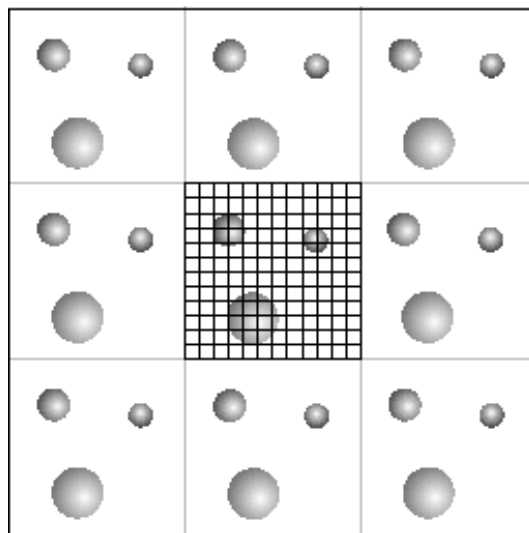


Figure 2: The periodic condition for an instanton ensemble sliced into 2-dimensional plane. We introduce the lattice on the center of the instanton ensemble to calculate the link variables with such a periodic condition for the sizes, positions color orientations of instantons.

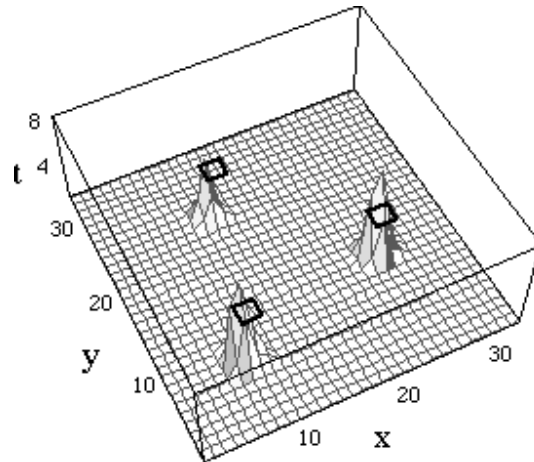


Figure 3-a: The dilute instanton system

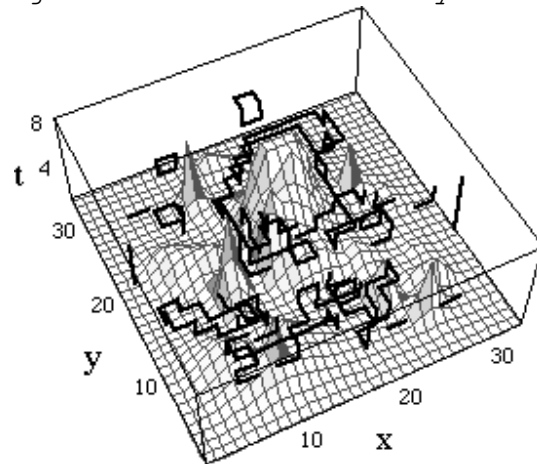


Figure 3-b: The dense instanton system

Figure 3: The local correlation between instantons and monopoles in the multi-instanton system. The thick lines denote monopole currents which appear at some time t . The bottom surface corresponds to the action density of instantons $s(x;y)$ at a certain time slice. Here, we show monopole currents which are transformed by one "block-spin" on the $32^2 \times 8$ lattice with $a = 0.125\text{fm}$.

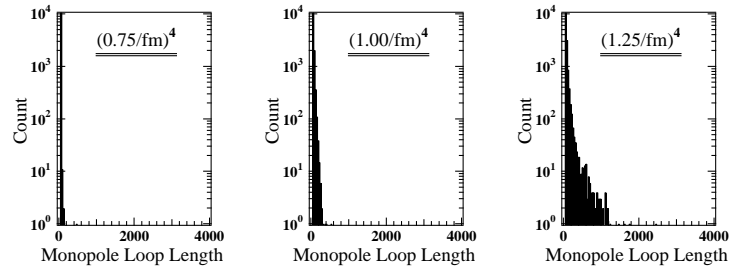


Figure 4-a: No "block-spin" transformation.
 (i) (ii) (iii)

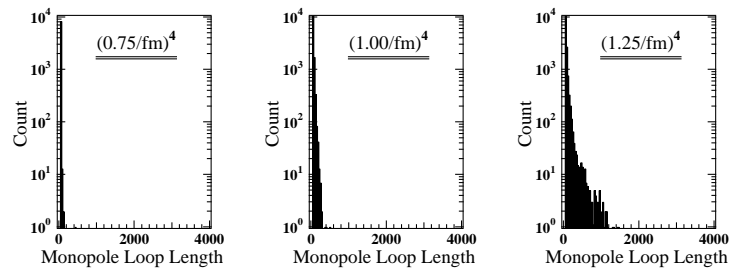


Figure 4-b: One "block-spin" transformation.
 (i) (ii) (iii)

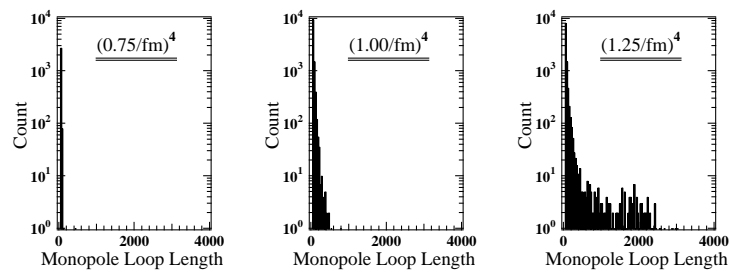


Figure 4-c: Two "block-spin" transformation.
 (i) (ii) (iii)

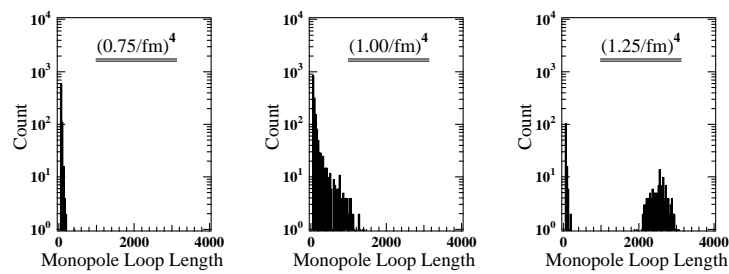


Figure 4-d: Three "block-spin" transformation.
 (i) (ii) (iii)

Figure 4: Histograms of monopole-loop lengths with various densities after the various "block-spin" transformations in the $\beta = 5$ case.

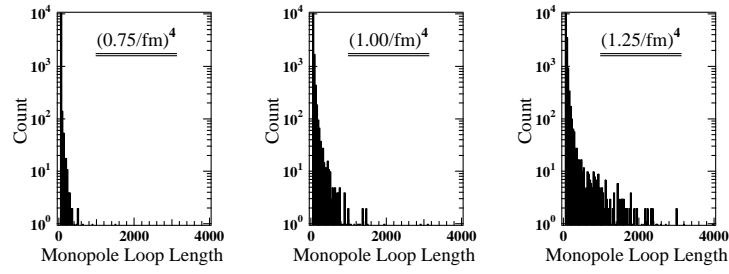


Figure 5-a: No "block-spin" transformation.
 (i) (ii) (iii)

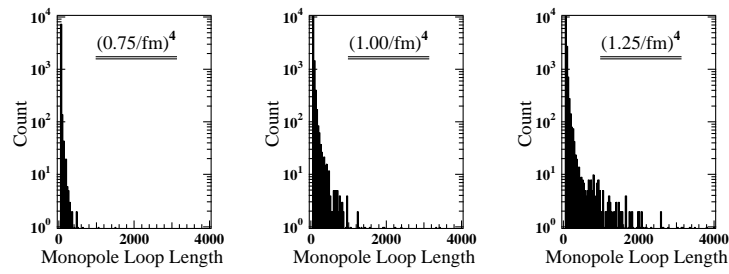


Figure 5-b: One "block-spin" transformation.
 (i) (ii) (iii)

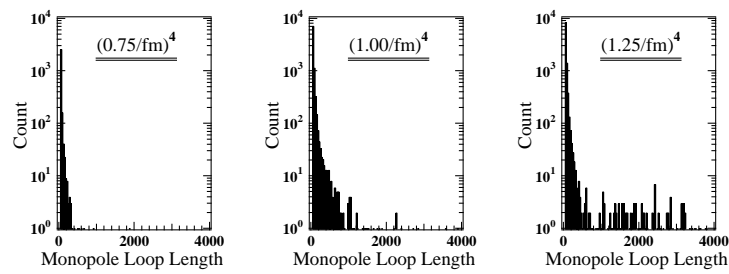


Figure 5-c: Two "block-spin" transformation.
 (i) (ii) (iii)

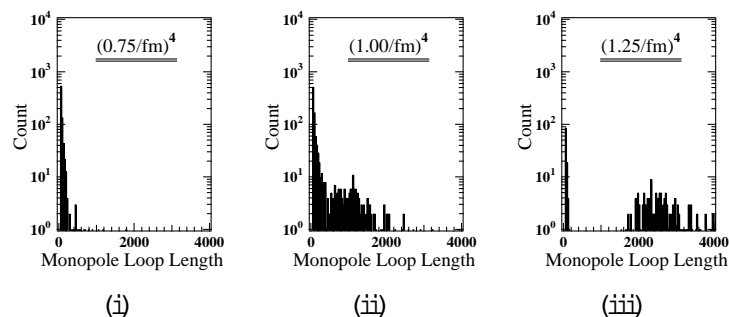


Figure 5-d: Three "block-spin" transformation.

Figure 5: Histograms of monopole-loop lengths with various densities after the various "block-spin" transformations in the $\beta = 3$ case.

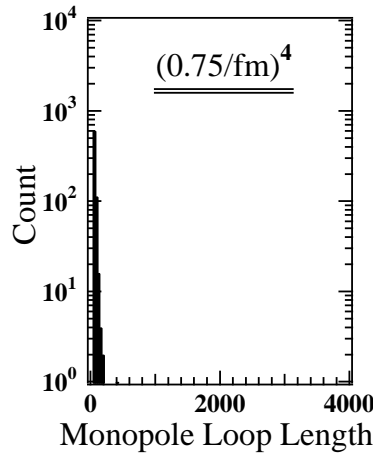


Figure 6-a:

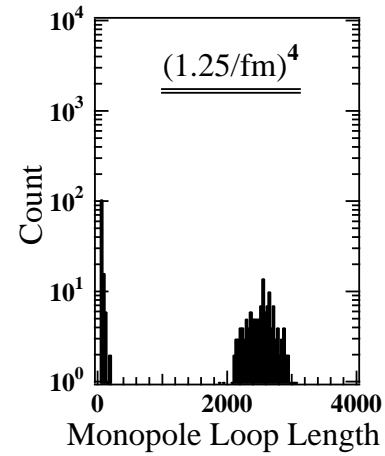


Figure 6-b:

Figure 6: The histograms of three "block-spin" transformed monopole-loop length in the multi-instanton system with $\beta = 5$. a) low instanton density and b) high instanton density.

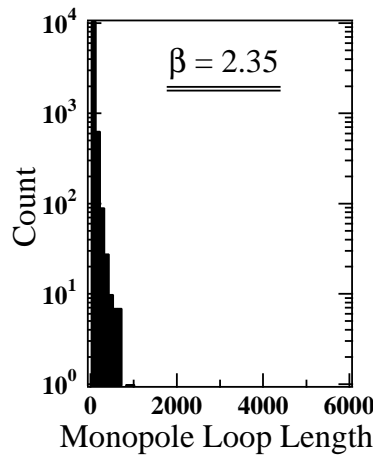


Figure 7-a:

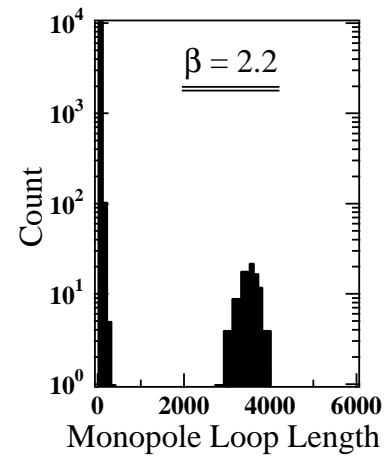


Figure 7-b:

Figure 7: The histogram of monopole-loop length in finite temperature lattice QCD . c) high temperature and d) low temperature.

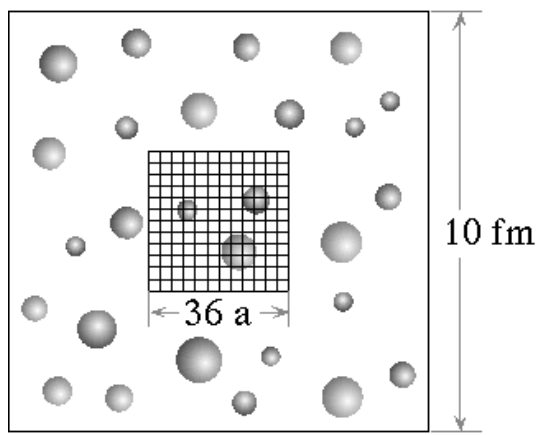


Figure 8: Random instanton configuration without the periodic boundary condition for sizes, positions and color orientations of instantons sliced into 2-dimensional plane. We introduce the lattice on the center of the random instanton ensemble. a denotes the lattice unit and 36 corresponds to the number of lattice point in each time-space direction.

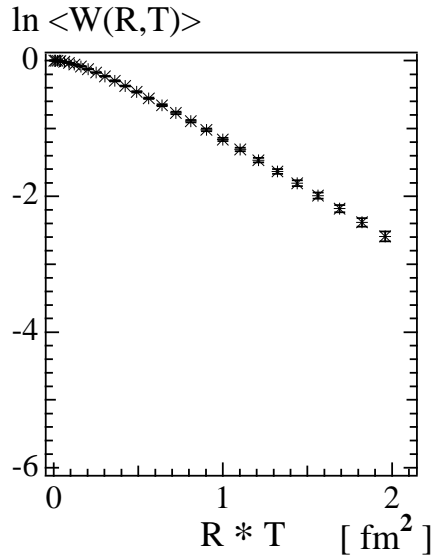


Figure 9: The Wilson loop behavior in the multi-instanton system as a function of the area $R \cdot T$ with the infrared instanton size distribution $\gamma = 5$.

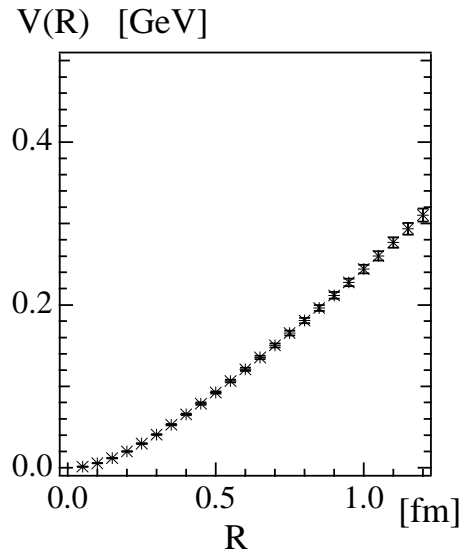


Figure 10: The static potential in the multi-instanton system as a function of the distance R with the infrared instanton size distribution $\gamma = 5$.

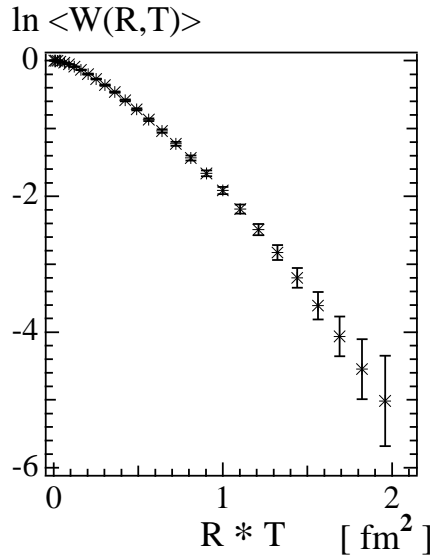


Figure 11: The Wilson loop behavior in the multi-instanton system as a function of the area $R \cdot T$ with the infrared instanton size distribution $\gamma = 3$.

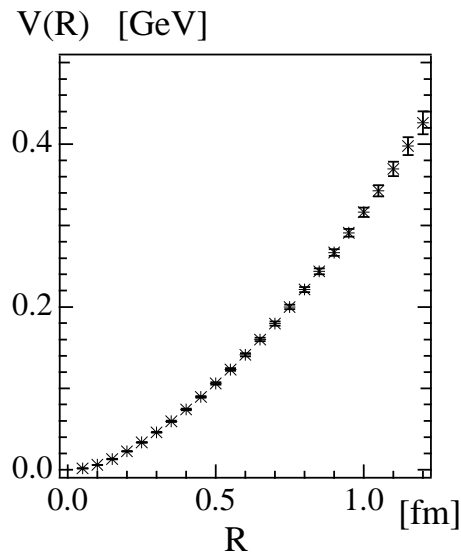


Figure 12: The static potential in the multi-instanton system as a function of the distance R with the infrared instanton size distribution $\gamma = 3$.

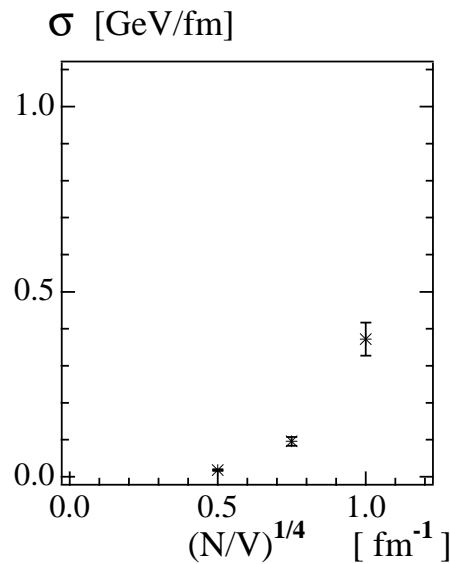


Figure 13: The string tension as a function of the in-stanton density $(N/V)^{1/4}$ with the infrared instanton size distribution $\gamma = 5$.

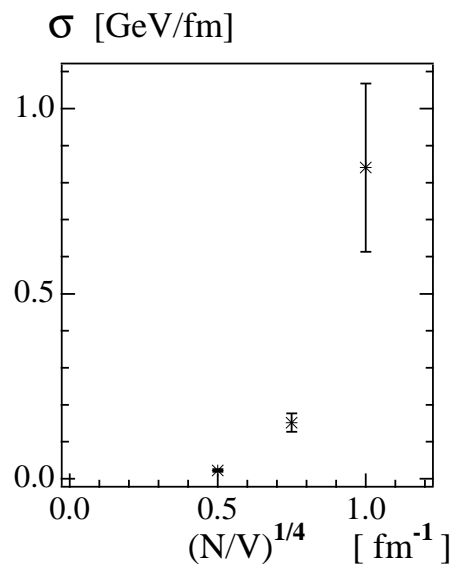


Figure 14: The string tension as a function of the in-stanton density $(N/V)^{1/4}$ with the infrared instanton size distribution $\gamma = 3$.